Proceedings of the ASME 2018 International Mechanical Engineering Congress & Exposition
IMECE 2018
November 9-15, 2018, Pittsburgh, USA

IMECE2018-88257

STATISTICAL VOLUME ELEMENTS FOR THE CHARACTERIZATION OF ANGLE-DEPENDENT FRACTURE STRENGTHS

Justin M. Garrard*
Mechanical, Aerospace,
& Biomedical Engineering Dept.
University of Tennessee Space Institute
411 B.H. Goethert Pkwy.
Tullahoma, Tennessee 37388
Email: jgarrard@utsi.edu

Reza Abedi
Mechanical, Aerospace,
& Biomedical Engineering Dept.
University of Tennessee Space Institute
411 B.H. Goethert Pkwy.
Tullahoma, Tennessee 37388
Email: rabedi@utsi.edu

ABSTRACT

As a quasi-brittle material, the fracture response of rock is very sensitive to its microstructural defects. Herein, we use statistical volume elements (SVEs) to characterize rock fracture strength at the mesoscale, based on the distribution of microcracks at the microscale. The use of SVEs ensures that the material randomness is maintained upon "averaging" of microscale features. Certain fracture strengths, such as uniaxial tensile strength, uniaxial hydrostatic strength, shear strength, and uniaxial compressive strength, are obtained and characterized for different angles of loading. Thus, a material with anisotropic fracture strength can be characterized. Statistics of the characterized strengths are analyzed, as well as their auto- and cross-correlation functions of these random fields to shed light on the length scales, relative to the volume element size, at which homogenized properties vary. While crack interaction is not included, the analysis provides insight on the distribution and correlation of different strengths. Finally, the asynchronous space-time discontinuous Galerkin method is used for macroscopic fracture analyses of two rock domains homogenized by SVEs.

INTRODUCTION

The response of quasi-brittle materials under loading is determined by the microscale distribution of cracks and other defects. Due to the lack of energy dissipative mechanisms within these materials, microcrack stress concentrations are not balanced as in ductile materials [1, 2]. Crack pattern variability under the same loading [3], ultimate strength uncertainties [4, 5], and other material heterogeneities are a consequence of the sensitivity of quasi-brittle materials to these microstructural flaws. The *size effect*, wherein the fracture strength decreases as the size of the specimen increases, is a direct result of these flaws. Thus, networks of microcracks can lead to very different fracture patterns even under the same loading and geometry settings [3] for different material samples.

Consequently, modeling these materials requires a consideration of these heterogeneities and anisotropy. When performing a fracture analysis, the heterogeneities can be implemented using either implicit or explicit methods. Explicit methods directly introduce these heterogeneities into the solution scheme. One well-known explicit method is lattice modeling [6], where a lattice of elements is used to represent a particle network connected by springs. One major drawback to these implicit methods are the small space and time-scales required to directly resolve the defects in the solution. To resolve this issue, an implicit method may be used which does not directly include microstructural details in the analysis, and instead incorporates their overall effect without requiring the short scales necessary for explicit methods.

Weibull's weakest link method [7, 8] is an example of an implicit method which has proven very effective in capturing the size effect and stochastic variations in fracture response. The authors have employed the Weibull model for multiple purposes,

*Address all correspondence to this author.

including capturing statistical fracture response of rock in hydraulic fracturing [9], fracture under dynamic compressive loading [10], and in fragmentation studies [11]. The Weibull model provides only a phenomenological characterization of fracture strength, however, and lacks the direct connection to the material microstructure.

Therefore, a homogenization approach is desired which resolves this issue with the Weibull method. Homogenization approaches derive the macroscopic properties of the material by solving the problem in a *Volume Element* (VE). Similar approaches can be used to calibrate certain fracture models, for example, [12–15]. A *Representative Volume Element* (RVE) is a class of VEs which is a subset of the overall domain, but still appreciably larger than the microscale features. Because the RVE is so much larger than the microscale, the RVE approaches the homogeneous macro response of the domain, while containing a large number of heterogeneities. Because of the RVE's size, the RVE loses the spatial inhomogeneity and sample to sample variation expected for microscale features. In order to capture these inhomogeneities, another class of VE known as a *Statistical Volume Element* (SVE) is used. The SVE, which is small enough to capture the aforementioned microscale features, have been used to capture both elastic [16–18] and fracture responses [19]. The authors are referred to [20, 21] for a more detailed comparison of RVEs and SVEs. Moreover, the SVE has been formulated for fracture in quasi-brittle materials by the authors in [22], showing the importance of incorporating inhomogeneity in fracture strength.

For rock, due to the existence of bedding plane, modeling anisotropy in fracture and elastic properties is as important as modeling inhomogeneities. Once the anisotropy of fracture strength is characterized, there are two main approaches to incorporate them in a macroscopic continuum model: [23,24] used a second order *microstructure tensor*, in additional to commonly used invariants of stress tensor, to define a general failure criterion. In contrast to the the aforementioned bulk failure model, well-known interfacial models such as Mohr-Coulomb or Hoek-Brown [25] are made angle-dependent in [26–28] by assigning different tensile strengths, friction coefficient, *etc.* for different angles of loading.

In this work, we adopt the latter approach, in that for any potential angle of loading we characterize different fracture strength parameters. This work build on our previous work in [22, 29] where SVEs containing microcracks are analyzed to derive fracture properties. However, unlike previous work were tensile strength was modeled as an angle-independent field, we derive uniaxial tensile strength of SVEs for arbitrary loading angles. Second, to have a more realistic characterization of fracture response on a fracture plane, other fracture strengths such as compressive and shear strengths are also determined for a given direction. Third, fracture under compressive stress state due to strong frictional sliding is modeled herein.

Angular dependent fracture strengths are developed in the next section, and the statistics of these strengths analyzed in the Numerical Results section for both an isotropic and angularly biased anisotropic domain. Covariance functions are used to determine how the calculated fracture strengths change in relation to itself and each other when traversing through the space-angle domain. Afterwards, an asynchronous spacetime Galerkin finite element method is used to analyze the fracture response of these domains with the applied random fracture strength fields.

FORMULATION

This section defines the statistical volume element approach for defining fracture strength in a quasi-brittle domain with respect to varying loading angle. Subsection one details how to characterize a domain with distributed microcracks using RVEs and SVEs. The next subsection then describes the process to calculate the angular-dependent fracture strength field. Next, a description of the covariance function and its use to determine the correlation of the fracture strength random fields is shown. Finally, the *asynchronous Spacetime Discontinuous Galerkin* (aSDG) method is detailed for performing dynamic fracture simulations within the given quasi-brittle domains.

RVE and SVE Definition

As mentioned in the Introduction, a *representative volume element* (RVE) of a given domain is large enough to represent the multitude of micro-heterogeneities within the domain, while still being sufficiently smaller than the overall structure. When the size of the volume element is reduced, the RVE approaches the *statistical volume element* (SVE) regime. The characteristic size of the SVE L_{SVE} is smaller than the overall size of the domain of interest L_M, ($L_{SVE} \ll L_M$), and the ratio of the SVE size to the size of the average microcrack length must be small enough that the SVE does not approach the RVE limit, β=L_{SVE}/l_m. Randomness is lost as the ratio β approaches infinity. This size effect is investigated further in the Numerical Results section.

For this paper, a 32x32 meter domain representing an RVE sample of a larger domain is selected. The domain is sampled with a uniform grid consisting of the center points of the respective SVEs. The grid spacing, $S = L_{SVE}/n$, is a function of the SVE size, L_{SVE}, and a grid line spacing variable, n, that is chosen such that the SVEs overlap by some amount such that the entire domain is sampled with sufficient resolution regardless of SVE size or shape. For every SVE sampled, the given microcracks which intersect with the SVE are analyzed and used to determine the angularly dependent fracture strength field, as described in the following section.

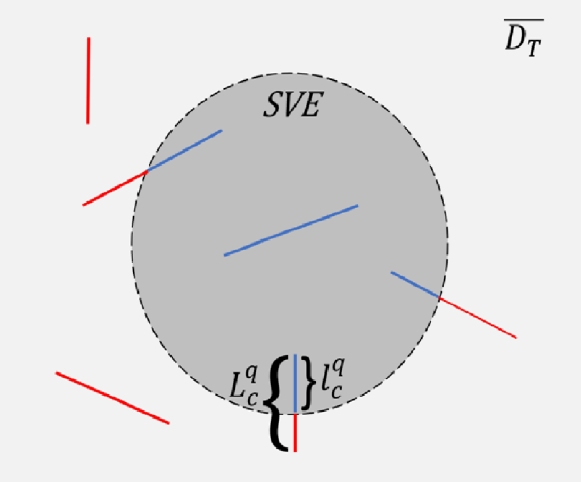

FIGURE 1. CRACKS WITHIN SVE FOR FRACTURE STRENGTH CALCULATION

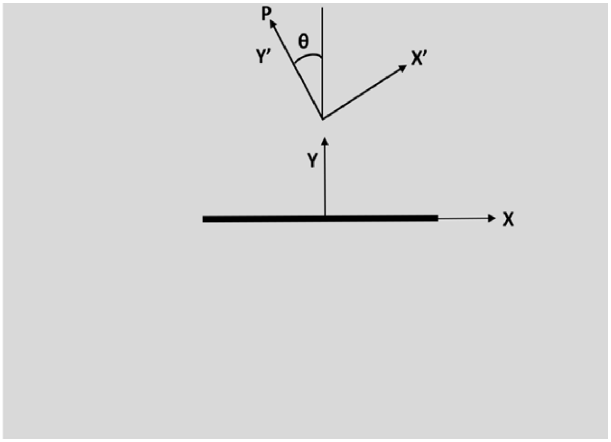

FIGURE 2. CRACK IN INFINITE DOMAIN WITH VARYING LOAD ANGLE

Fracture Strength Calculations

Within the statistical volume element, all possible intersecting microcracks are considered. For this work, a circular SVE shape was chosen. Cracks both completely encircled by the SVE domain or only partially intersecting are considered. If no crack intersects the SVE, a maximum fracture strength is assigned to the SVE based on a crack of minimum length. For Figure 1, all cracks within the circle which are analyzed are blue, while those outside the SVE which are ignored are red.

For a crack of effective length a, the strength is calculated from *Linear Elastic Fracture Mechanics* (LEFM) principles. The first assumption utilizing this approach is that upon the propagation of the first microcrack, the SVE is considered to be completely failed. Next, linear elasticity may be assumed for quasi-brittle fracture within RVEs and SVEs because the load at which the material response begins to deviate from this linear behavior is close to the volume elements failure strength [30]. Therefore, utilizing the LEFM approach, the point of departure for linear elasticity is when the stress intensity factor for the most critical crack within the SVE reaches the fracture toughness. To approximate the stress intensity factor, a crack in an infinite domain is used. One major drawback of this assumption is that crack interactions are ignored; however, the assumption is believed to still represent the overall anisotropy of the macroscopic fracture field.

The critical energy release rate G_C is used to calculate the fracture strength. The angle of loading is varied, and the fracture strength is calculated at periodic intervals. Figure 2 is depicts how the angle of loading, θ, changes for the calculation of the given strength. The loading angle at degree zero is perpendicular to the crack direction, opening the crack and resulting in the angle of minimum fracture strength. Loading angles of 90 degrees are parallel to the crack tip, which results in the maximum fracture strength for the given loading angle range.

Utilizing a mixed mode fracture strength calculation, the traction loading P is applied, resulting in the stress components $\sigma_{y'y'}$, $\sigma_{x'x'}$ and $\sigma_{x'y'}$. Solving the mixed mode fracture equations yields the following equations for tensile (S_N), shear (S_S), compressive (S_C), and hydrostatic tensile (S_{HN}) strengths:

$$S_S\sqrt{\frac{\pi a}{G_C E'}} = \begin{cases} 1, & -\frac{\pi}{2} < \theta < 0 \\ \frac{1}{\cos 2\theta - kL2\theta}, & 0 < \theta < (\frac{\pi}{4} - \frac{\phi}{2}) \\ \infty, & (\frac{\pi}{4} - \frac{\phi}{2}) < \theta < (\frac{\pi}{4} + \frac{\phi}{2}) \\ \frac{1}{-\cos 2\theta - kL2\theta}, & (\frac{\pi}{4} + \frac{\phi}{2}) < \theta < \frac{\pi}{2} \end{cases} \tag{1a}$$

$$S_C\sqrt{\frac{\pi a}{G_C E'}} = \begin{cases} \frac{1}{-\cos\theta(\sin\theta + k\cos\theta)}, & -\frac{\pi}{2} < \theta < -\phi \\ \infty, & -\phi < \theta < \phi \\ \frac{1}{\cos\theta(\sin\theta - k\cos\theta)}, & -\phi < \theta < \frac{\pi}{2} \end{cases} \tag{1b}$$

$$S_N\sqrt{\frac{\pi a}{G_C E'}} = \frac{1}{|\cos\theta|} \tag{1c}$$

$$S_{NH}\sqrt{\frac{\pi a}{G_C E'}} = 1 \tag{1d}$$

where k and $\phi = \tan^{-1}(k)$ are friction and friction angle, respectively, and a is the half-crack length. The stiffness parameter E' is equal to $E/(1-\nu^2)$ and E for plane strain and plain stress conditions, respectively. The friction coefficient appears in equations as under compressive stress state ($\sigma_{y'y'} < 0$), mode one stress intensity factor, K_I, is zero, and mode two fracture can occur only if Coulomb slip condition holds on crack surfaces.

The maximum strength assigned to each SVE is equivalent

to the strength at angle θ equal to zero with the minimum allowable crack length a that is processed. When looping over each crack within the SVE domain, the minimum calculated strength is retained for each of the three angular dependent strength fields (plus the angular independent hydrostatic strength) and associated to that specific SVE. These fields of minimum fracture strengths are then created which represents the anisotropy and inhomogeneity of the structure.

Covariance and Correlation Functions

The covariance of a random field is a description of how the variable changes within the field. For the given anisotropic problem, there are multiple parameters to consider. The fracture strength field changes spatially, angularly, and between each specified strength. The covariance can be calculated between two variables X and Y utilizing equation 2, where μ is the variable mean.

$$cov(X,Y) = E(X-\mu_X)E(Y-\mu_Y) \tag{2}$$

After the covariance function is calculated, the correlation of the two variables can then be calculated. The Pearson correlation coefficient, referred to as *Pearson's r*, is used to calculate how correlated the two variables are. If r is equal to $+1$, then the two variables are completely positively linearly correlated, while if equal to -1 the variables are completely negatively linearly correlated. An r value equal to 0 means that the two variables are not linearly correlated at all. The correlation function is calculated using equation 3 utilizing the covariance function and the standard deviations of the two variables, denoted by σ. These two covariance and correlation functions are then used to determine how the random field is related. This can then be used to develop statistically consistent random fields using the *Karhunen-Loeve* (KL) method. Statistically consistent random fields are crucial to developing the efficient *stochastic partial differential equations*, which can be solved using methods detailed in [31].

$$corr(X,Y) = \frac{cov(X,Y)}{\sigma_x \sigma_y} \tag{3}$$

NUMERICAL RESULTS

The numerical results will be presented in order of the two different microcrack distributions, one isotropic and one anisotropic, developed for this work. For each microcrack distribution, the domain $\bar{D}$ is centered at x_{center} = (0,0) and spans 32 meters in both $\vec{x}$ and $\vec{y}$ directions, *i.e.,* the domain spans from $x \in \bar{D} = [-16,-16]$ to $[16,16]$. Each domain microcrack distribution was created using a Weibull distribution for crack length with *Weibull shape parameter* $m = 4$, *Weibull minimum value* $\gamma = 0.0755885$ m, and *Weibull scale* $\eta = 0.137259$ m. The isotropic domain has a uniform crack distribution between $[0,\pi]$ and has no angular bias.

The anisotropic crack distribution is biased between -25 and -15 degrees, *i.e.,* the domain has a mean angle of -20 degrees with a 10 degree span. This corresponds to a field with an orientation-dependent fracture strength that should be weakest at -20 degrees and strongest $\pm$ 90 degrees from the angle corresponding to min value, *i.e.,* at angles 70° and -110°. Material properties used for this analysis are Young's modulus $E = 65$ GPa, mass density $\rho = 2600$ kg/m^3, and Poisson's ratio $\nu = 0.3$. For both isotropic and anisotropic crack distributions, the mean crack length in the domain is 0.2 m with a standard deviation of 0.035 m. The minimum allowable crack length used to determine the maximum fracture strength is 0.02 m.

Isotropic Domain

As detailed above, the isotropic domain contains a uniform crack distribution between $[0,2\pi]$. Therefore, the domain is angularly unbiased. The process detailed in the formulation section was used to calculate the random fracture strength field for SVE sizes of 1, 2, 4, and 8 m SVE lengths. The loading angle θ was varied from $[0,\pi]$ with a spacing of five degrees within this range. Applying LEFM principles, the minimum uniaxial, tensile, shear, and compressive fracture strengths are calculated for every crack which intersected or were contained in an SVE.

From Figure 3, the impact of *size effect* can be seen. As the SVE size decreases, the isotropic random field fracture strength decreases and greater homogeneity is seen. The minimum uniaxial strength is taken over all loading angles around an SVE. This figure demonstrates that as the SVE size increases, *i.e.,* as it approaches the RVE size limit, the rock response becomes more homogeneous, represented by weaker minimum strengths.

Another interesting study is analyzing the rock anisotropy, where for a given point and SVE size the variation of fracture strength is measured for different loading angles. The anisotropy measure is defined as the standard deviation in loading angle for each SVE divided by the mean value. This is then calculated for each fracture strength field. This anisotropy measure is thus higher whenever the standard deviation of the fracture strength in angle is greater relative to the mean value.

Figure 4 shows the spatial distribution of anisotropic measure for S_N for different SVE sizes. Note that the color bars are not normalized. Therefore, it can be shown that the smaller the SVE size, the higher the level of anisotropy even for a isotropic domain. For a 1x1 SVE, the maximum measure of anisotropy is greater than one, while for SVEs of size 8x8, the maximum measure of anisotropy is only about 0.1. This again shows that as the SVE size increases, the variations in fracture strength, in space in Figure 3 and angle in Figure 4, decrease considerably.

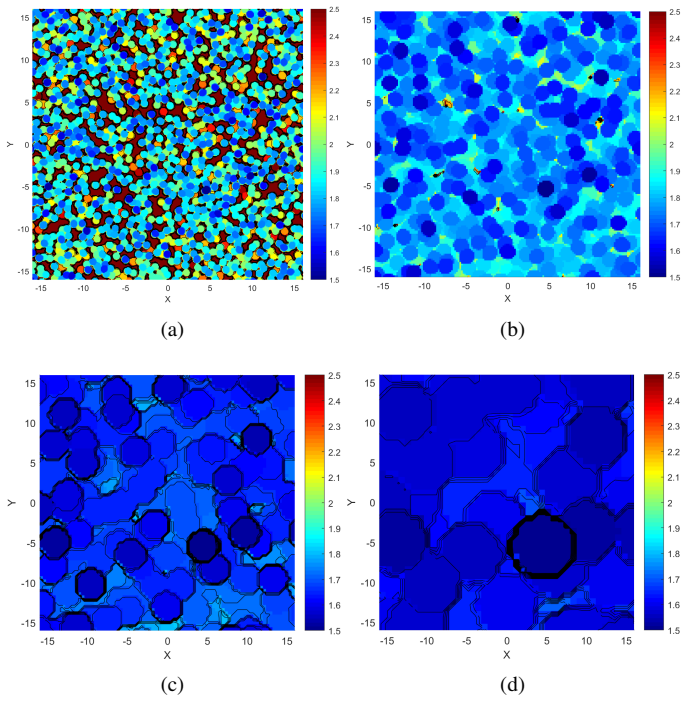

FIGURE 3. MINIMUM UNIAXIAL STRENGTH S_N FOR SVE SIZES L_{SVE} = (a) 1X1, (b) 2X2, (c) 4X4, AND (d) 8X8

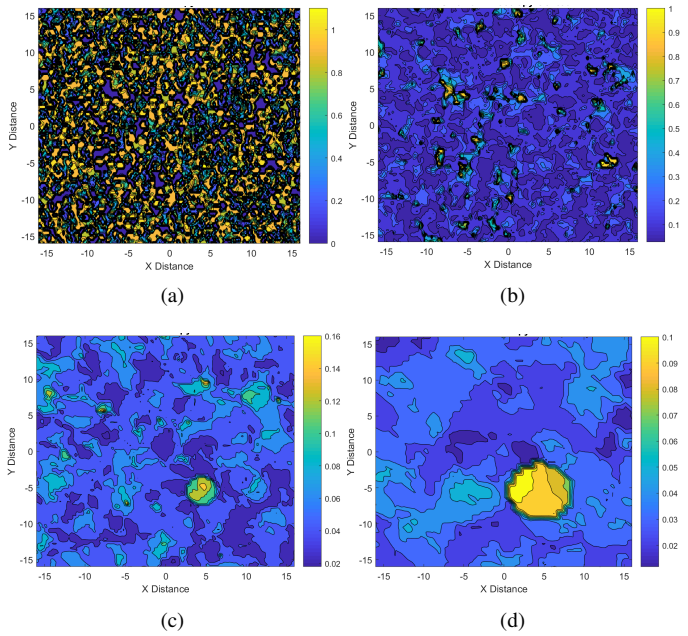

FIGURE 4. UNIAXIAL STRENGTH S_N ANISOTROPY MEASURE FOR L_{SVE} = (a) 1X1, (b) 2X2, (c) 4X4, AND (d) 8X8

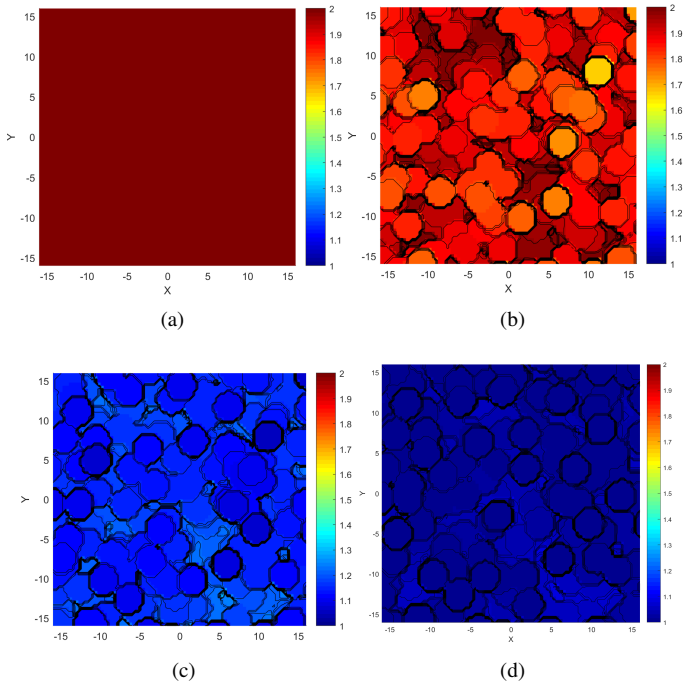

FIGURE 5. ANISOTROPIC DOMAIN UNIAXIAL FRACTURE STRENGTH S_N FOR VARYING θ = (a) 70 DEG, (b) 100 DEG, (c) 130 DEG, AND (d) 160 DEG

Anisotropic Domain

The anisotropic domain contains an angular bias about -20 degrees. Therefore, the minimum fracture strength is biased towards -20 degrees and maximum is biased about 70 degrees. Since the fracture strength is equivalent when the loading angle is shifted 180 degrees, -20 degrees is equivalent to 160 degrees, which should also show a minimum. Figure 5 shows that this is true. 70 degrees is the maximum strength, and progressively gets smaller the further away you get from the angle of maximum strength. Thus, the angular bias of the domain is made obvious. Also, as expected, the measure of anisotropy shown in Figure 6 for the SVE size 4x4 is uniformly high for the anisotropic domain, all approximately one.

Correlation and Covariance Functions

As detailed in the Formulation section, the correlation and covariance functions describes how the random field is related between two different points in the field. For these domains, the field can change spatially, angularly, and with strength. Aside from the physical perspective obtained by understanding various types of correlation of these random fields, the covariance function in particular is used in generating random fields in many statistical methods such as the *Karhunen-Loeve* method. The realized random fields for material properties eventually serve as

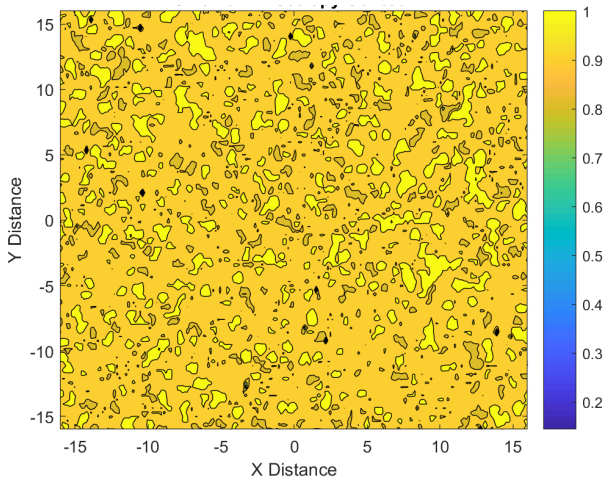

FIGURE 6. UNIAXIAL FRACTURE STRENGTH S_N ANISTROPY MEASURE FOR ANISTROPIC DOMAIN AND SVE SIZE 4x4

random parameters for a *stochastic partial differential equation* (SPDE) for the elastodynamic fracture problem. Therefore, this subsection will detail the correlations developed between the different strength fields and loading angles for both domains, and the covariance random field results are presented and discussed.

Correlation of Different Fracture Strengths. Applying the covariance and correlation functions between the individual fracture strength fields yields the R coefficient detailing the correlation between S_{HN}, S_N, S_S, and S_C for both the isotropic and anisotropic domains. Since the anisotropic domain has a strong angular bias, both the mean and min in angle fracture strengths were analyzed and shown in tables 1 and 2. The angular bias leads to a higher correlation between the min and mean fields, while reducing the correlation between the angular dependent S_N, S_S, and S_C strengths to the angular independent S_{HN} strength. All the minimum strength fields remain highly correlated between the two domains, while the correlation between the mean and minimum fields decrease within the anisotropic domain, another indication of the anisotropic angular biased nature of the domain.

Correlation of Different Angles. While the previous section discussed the correlation of the individual fracture strength fields, this section will detail the correlation in angle of a single strength field, S_{NA}. Figure 7 shows the isotropic domain. There is a strong correlation with the field to itself, which slowly tapers off as the delta between the angles increases. The profile remains uniform throughout, and since the load repeats itself past 180 degrees, the figure shows the increasing correlation at the extremes ($\theta = \pi$). Figure 8 shows the results for the

TABLE 1. PEARSON'S R COEFFICIENT FOR ISOTROPIC FRACTURE STRENGTH FIELDS

	S_{HN}	$S_{N,MN}$	$S_{S,MN}$	$S_{C,MN}$	$S_{N,MIN}$	$S_{S,MIN}$	$S_{C,MIN}$
S_{HN}	1	0.717	0.903	0.354	0.999	1	0.996
$S_{N,MN}$	0.717	1	0.893	0.619	0.717	0.717	0.713
$S_{S,MN}$	0.903	0.893	1	0.482	0.903	0.903	0.897
$S_{C,MN}$	0.354	0.619	0.482	1	0.354	0.354	0.353
$S_{N,MIN}$	0.999	0.717	0.903	0.354	1	0.999	0.995
$S_{S,MIN}$	1	0.717	0.903	0.354	0.999	1	0.996
$S_{C,MIN}$	0.996	0.713	0.897	0.352	0.995	0.996	1

TABLE 2. PEARSON'S R COEFFICIENT FOR ANISOTROPIC FRACTURE STRENGTH FIELDS

	S_{HN}	$S_{N,MN}$	$S_{S,MN}$	$S_{C,MN}$	$S_{N,MIN}$	$S_{S,MIN}$	$S_{C,MIN}$
S_{HN}	1	0.582	0.433	0.382	0.999	1	0.993
$S_{N,MN}$	0.582	1	0.839	0.933	0.584	0.582	0.563
$S_{S,MN}$	0.433	0.839	1	0.917	0.435	0.433	0.412
$S_{C,MN}$	0.382	0.933	0.917	1	0.384	0.382	0.360
$S_{N,MIN}$	0.999	0.584	0.434	0.384	1	0.999	0.992
$S_{S,MIN}$	1	0.582	0.433	0.382	0.999	1	0.993
$S_{C,MIN}$	0.993	0.563	0.412	0.360	0.992	0.993	1

anisotropic domain. For angle θ = 70 degrees, the location of maximum strength, there is a sharp increase in correlation that does not smoothly taper off as with the isotropic domain. A reduced, wider correlation band is seen across all other angles.

Spatial Covariance. Figures 9 and 10 show the spatial covariance field for the S_{NA} isotropic and anisotropic domain fields, respectively. As can be shown, the covariance of the field indicates the field is only strongly related close to the specified point in both domains. It is proposed that a spherical covariance function $cov = e^{\frac{-r^2}{d^2}}$ be used to approximate the covariance field, where r is the distance away from the point, and d is the SVE size, L_{SVE}.

Space-Angle Covariance. Space-angle covariance not only traverses the domain in space, but throughout the space-angle domain. The horizontal axis in Figures 11 and 12 corresponds to the spatial distance between two points along a given direction in space (X, Y) plane, while the vertical axes is the difference of these two points in terms of the angle at which fracture strength is measured; the fracture angle of one of these points is considered at the loading angle zero, while for the other, strength

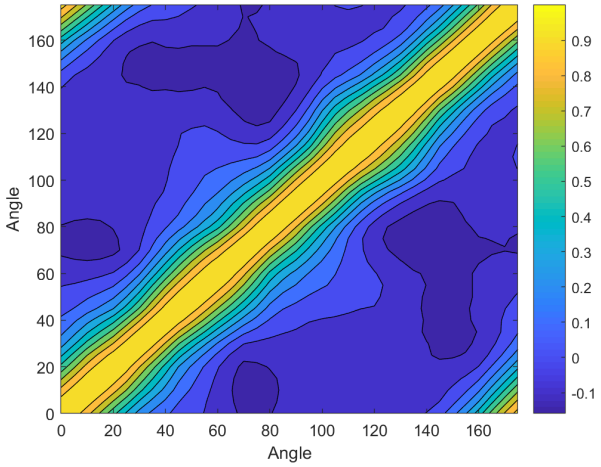

FIGURE 7. UNIAXIAL STRENGTH S_N CORRELATION IN ANGLE ISOTROPIC DOMAIN

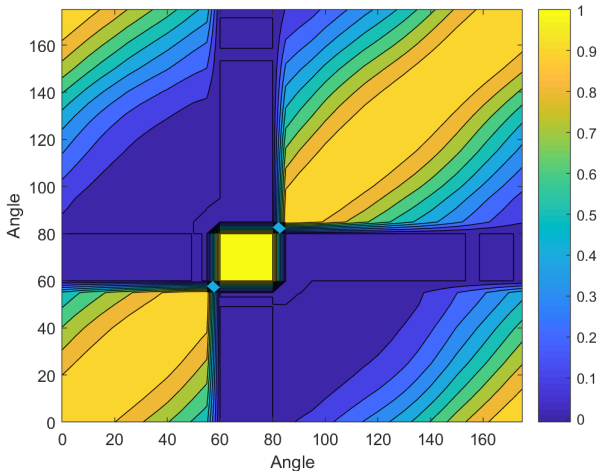

FIGURE 8. UNIAXIAL STRENGTH S_N CORRELATION IN ANGLE ANISOTROPIC DOMAIN

at angle θ is considered. For the distance in space, X and Y are selected such that the spatial domain is being traversed at an angle of -20 degrees from the base point, which is the angle of minimum strength. In the isotropic domain, there is no obvious angular bias shown The anisotropic plot shows a distinct band about the angle of maximum strength wherein the covariance is extremely low at $\theta = 70$ degrees, the angle of maximum strength.

aSDG Fracture Simulation Results

The asynchronous spacetime discontinuous Galerkin finite element method formulated for elastodynamic problems [32] is used to simulate the fracture within the anisotropic domain. The method employs discontinuous basis functions across finite element boundaries and directly discretizes spacetime using non-uniform grids that satisfies a special causality constraint [33]. In lieu of traditional *traction separation relations* (TSRs), an interfacial damage model [11] is used to model damage evolution on crack surfaces. For mode II fracture under compressive loads, which is common in rock as for example for the problem considered herein, dynamic contact–stick and contact–slip modes [34] are incorporated in the model. The use of dual error indicators for controlling energy error in the bulk and on fracture surfaces [35], *h*-adaptivity in spacetime [36], and alignment of element boundaries with arbitrary crack propagation directions [11, 37] are all essential in capturing complexing fracture patterns such as those

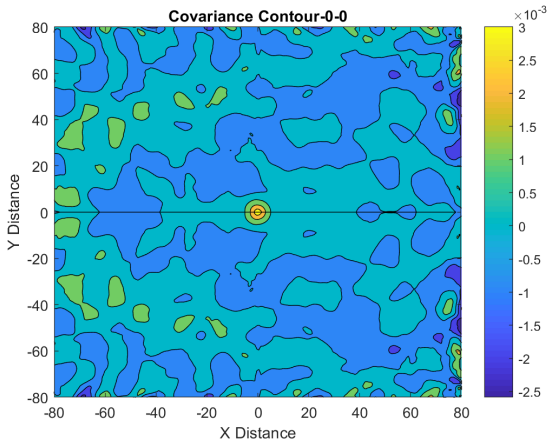

FIGURE 9. COVARIANCE FUNCTION IN SPACE ISOTROPIC DOMAIN Please zoom in to a [-25, 25] x [-25, 25] region, same for the next figure.

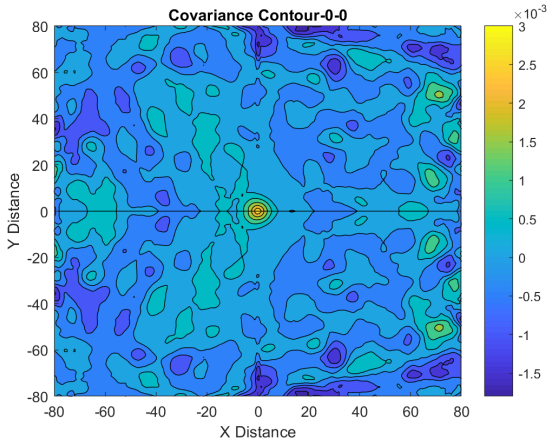

FIGURE 10. COVARIANCE FUNCTION IN SPACE ANISOTROPIC DOMAIN

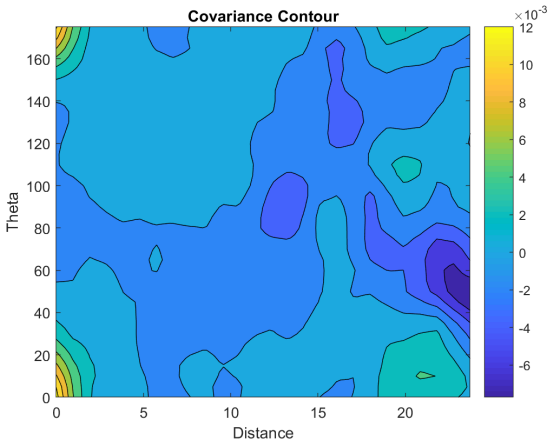

FIGURE 11. COVARIANCE FUNCTION IN SPACE-ANGLE ISOTROPIC DOMAIN

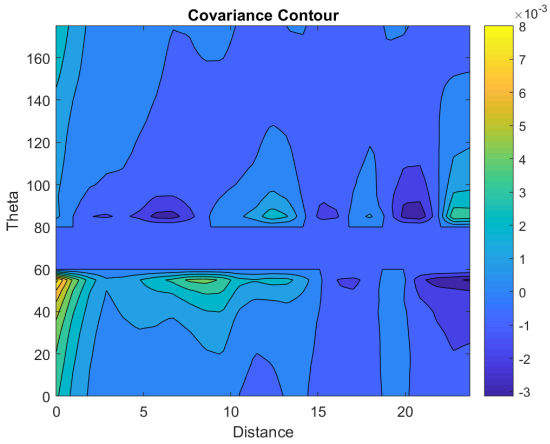

FIGURE 12. COVARIANCE FUNCTION IN SPACE-ANGLE ANISOTROPIC DOMAIN

reported in Figures 13 and 14.

The fracture simulations demonstrate the effect of rock fracture strength anisotropy in induced fracture pattern under a compressive load. The computational domain is loaded compressively in the X-Direction until failure. The initial and boundary conditions are specified such that, before the occurrence of the first crack, they generate a spatially uniform and a temporally increasing negative strain field ε_{XX}, while ε_{XY} and ε_{YY} are zero. The fracture strength field is inhomogeneous, as for example see in Figure 3, the generated random fields are spatially variant. In addition, the uniaxial tensile strength S_N used for these simulations, by construction is angle-dependent. So, the sampled values for S_N are both space and angle dependent. The result in Figure 13 corresponds to the rock sample with no angular bias, while

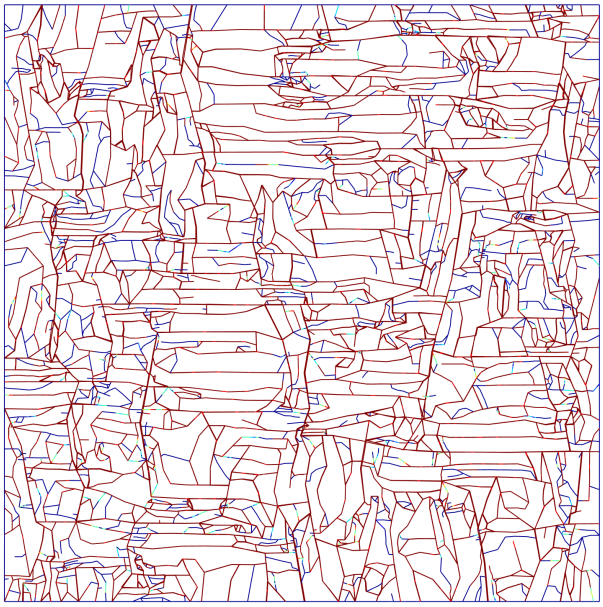

FIGURE 13. DYNAMIC SIMULATION OF ISOTROPIC FRACTURE FIELD

in Figure 14 the homogenized strengths for the domain with -20 degrees angular bias is used for macroscopic fracture simulation. As evident when anisotropy is included, the crack pattern will be much different than that if it is left out. This shows how a complex fracture pattern can be completely inaccurate if angular bias (anisotropy) is not included in the model. Assumptions about how cracks propagate in a given domain can be very flawed without including anisotropy. Regardless, including spatial inhomogeneity is more realistic than assuming the entire domain is homogeneous.

CONCLUSION

Angular dependency is crucial when performing quasi-brittle fracture simulations. Without including this anisotropy into the analysis, the model will miss the influence of weaker planes or regions within the domain. This will lead to an inaccurate analysis of the real strength and behavior of the material. Utilizing the *statistical volume element* (SVE) approach, a process was developed to introduce inhomogeneity and anisotropy into the solution to develop random fields of material properties. This process was repeated for varying loading angles between $[0, /pi]$ with four different SVE sizes. As the SVE size decreases, the measure of anisotropy in the model increased greatly, while larger SVEs approach the RVE limit and were homogeneous and contained very little anisotropy. The dynamic analyses by the aSDG method showed the importance of including inhomogeneity and anisotropy into the solution. Without anisotropy,

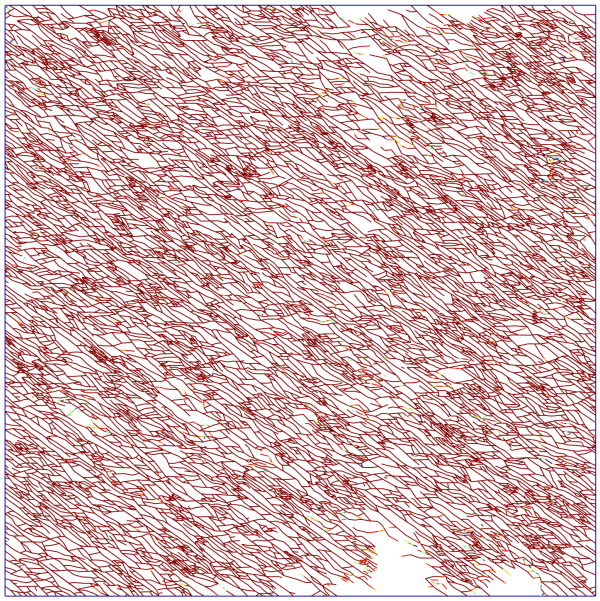

FIGURE 14. DYNAMIC SIMULATION OF ANISOTROPIC FRACTURE FIELD

the quasi-brittle material would be inaccurately assumed to be equally likely to fail in all directions under the same loading conditions without including these variables.

In future work, rather than assuming a certain probability distribution for crack lengths, we plan to use actual microcrack statistics of rocks such as those reported in [38] an more robust approaches for their generation [39]. In addition, similar to our previous work in [22, 29] we will use the *Karhunen-Loeve* (KL) method [40, 41] to realize random fields that are consistent with the statistics of homogenized SVEs. The addition of variability of strength in angle, and anisotropy of strength as in the angle-biased example, significantly complicates the realization of such random fields. The isotropic and anisotropic covariance and correlation functions obtained in Section allows the extension of KL method in [22, 29] for these more general problems.

ACKNOWLEDGMENT

The authors gratefully acknowledge partial support for this work via the U.S. National Science Foundation (NSF), CMMI - Mechanics of Materials and Structures (MoMS) program grant numbers 1538332 and 1654198.

REFERENCES

[1] Rinaldi, A., Krajcinovic, D., and Mastilovic, S., 2007. "Statistical damage mechanics and extreme value theory". *International Journal of Damage Mechanics,* ***16***(1), pp. 57–76.

[2] Genet, M., Couegnat, G., Tomsia, A., and Ritchie, R., 2014. "Scaling strength distributions in quasi-brittle materials from micro- to macro-scales: A computational approach to modeling nature-inspired structural ceramics". *Journal of the Mechanics and Physics of Solids,* ***68***(1), pp. 93–106.

[3] Al-Ostaz, A., and Jasiuk, I., 1997. "Crack initiation and propagation in materials with randomly distributed holes". *Engineering Fracture Mechanics,* ***58***(5-6), pp. 395–420.

[4] Kozicki, J., and Tejchman, J., 2007. "Effect of aggregate structure on fracture process in concrete using 2D lattice model". *Archives of Mechanics,* ***59***(4-5), pp. 365–84.

[5] Yin, X., Chen, W., To, A., McVeigh, C., and Liu, W. K., 2008. "Statistical volume element method for predicting microstructure–constitutive property relations". *Computer methods in applied mechanics and engineering,* ***197***(43-44), pp. 3516–29.

[6] Li, J., 2000. "Debonding of the interface as 'crack arrestor"'. *International Journal of Fracture,* ***105***(1), pp. 57–79.

[7] Weibull, W., 1939. "A statistical theory of the strength of materials". *R. Swed. Inst. Eng. Res.*, p. Res. 151.

[8] Weibull, W., 1951. "A statistical distribution function of wide applicability". *Journal of Applied Mechanics,* ***18***, pp. 293–297.

[9] Abedi, R., Omidi, O., and Clarke, P., 2016. "Numerical simulation of rock dynamic fracturing and failure including microscale material randomness". In Proceeding: 50th US Rock Mechanics/Geomechanics Symposium. ARMA 16-0531.

[10] Abedi, R., Haber, R., and Elbanna, A., 2017. "Mixed-mode dynamic crack propagation in rocks with contact-separation mode transitions". In Proceeding: 51th US Rock Mechanics/Geomechanics Symposium. ARMA 17-0679.

[11] Abedi, R., Haber, R. B., and Clarke, P. L., 2017. "Effect of random defects on dynamic fracture in quasi-brittle materials". *International Journal of Fracture,* ***208***(1-2), pp. 241–268.

[12] Taylor, L. M., Chen, E.-P., and Kuszmaul, J. S., 1986. "Microcrack-induced damage accumulation in brittle rock under dynamic loading". *Computer Methods in Applied Mechanics and Engineering,* ***55***(3), pp. 301 – 320.

[13] Homand-Etienne, F., Hoxha, D., and Shao, J., 1998. "A continuum damage constitutive law for brittle rocks". *Computers and Geotechnics,* ***22***(2), pp. 135–151.

[14] Shao, J., and Rudnicki, J., 2000. "A microcrack-based continuous damage model for brittle geomaterials". *Mechanics of Materials,* ***32***(10), pp. 607–619.

[15] Lu, Y., Elsworth, D., and Wang, L., 2013. "Microcrack-based coupled damage and flow modeling of fracturing evolution in permeable brittle rocks". *Computers and Geotech-*

nics, ***49***, pp. 226–44.

[16] Baxter, S. C., and Graham, L. L., 2000. "Characterization of random composites using moving-window technique". *Journal of Engineering Mechanics,* ***126***(4), pp. 389–397.

[17] Tregger, N., Corr, D., Graham-Brady, L., and Shah, S., 2006. "Modeling the effect of mesoscale randomness on concrete fracture". *Probabilistic Engineering Mechanics,* ***21***(3), pp. 217–225.

[18] Segurado, J., and LLorca, J., 2006. "Computational micromechanics of composites: The effect of particle spatial distribution". *Mechanics of Materials,* ***38***(8), pp. 873–883.

[19] Koyama, T., and Jing, L., 2007. "Effects of model scale and particle size on micro-mechanical properties and failure processes of rocks—a particle mechanics approach". *Engineering Analysis with Boundary Elements,* ***31***(5), pp. 458–472.

[20] Ostoja-Starzewski, M., 2002. "Microstructural randomness versus representative volume element in thermomechanics". *Journal of Applied Mechanics-Transactions of the ASME,* ***69***(1), pp. 25–35.

[21] Ostoja-Starzewski, M., 2006. "Material spatial randomness: From statistical to representative volume element". *Probabilistic Engineering Mechanics,* ***21***(2), pp. 112 – 132.

[22] Clarke, P., Abedi, R., Bahmani, B., Acton, K., and Baxter, S., 2017. "Effect of the spatial inhomogeneity of fracture strength on fracture pattern for quasi-brittle materials". In Proceedings of ASME 2017 International Mechanical Engineering Congress & Exposition IMECE 2017, p. V009T12A045 (9 pages). IMECE2017-71515.

[23] Pietruszczak, S., and Mroz, Z., 2000. "Formulation of anisotropic failure criteria incorporating a microstructure tensor". *Computers and Geotechnics,* ***26***(2), pp. 105–112.

[24] Pietruszczak, S., Lydzba, D., and Shao, J., 2002. "Modelling of inherent anisotropy in sedimentary rocks". *International Journal of Solids and Structures,* ***39***(3), pp. 637–648.

[25] Hoek, E., and Brown, T., 1980. *Underground Excavations in Rock*. Geotechnics and foundations. Taylor & Francis.

[26] Pietruszczak, S., and Mroz, Z., 2001. "On failure criteria for anisotropic cohesive-frictional materials". *International Journal for Numerical and Analytical Methods in Geomechanics,* ***25***(5), pp. 509–524.

[27] Lee, Y.-K., and Pietruszczak, S., 2008. "Application of critical plane approach to the prediction of strength anisotropy in transversely isotropic rock masses". *International Journal of Rock Mechanics and Mining Sciences,* ***45***(4), pp. 513–23.

[28] Shi, X., Yang, X., Meng, Y., and Li, G., 2016. "An anisotropic strength model for layered rocks considering planes of weakness". *Rock Mechanics and Rock Engineering,* ***49***(9), pp. 3783–92.

[29] Clarke, P., and Abedi, R., 2017. "Fracture modeling of rocks based on random field generation and simulation of inhomogeneous domains". In Proceeding: 51th US Rock Mechanics/Geomechanics Symposium. ARMA 17-0643.

[30] Nguyen, V. P., Lloberas-Valls, O., Stroeven, M., and Sluys, L. J., 2011. "Homogenization-based multiscale crack modelling: From micro-diffusive damage to macro-cracks". *Computer Methods in Applied Mechanics and Engineering,* ***200***(9), pp. 1220–36.

[31] Ghanem, R., and Spanos, P., 1991. *Stochastic finite elements: a spectral approach*. Springer-Verlag.

[32] Abedi, R., Haber, R. B., and Petracovici, B., 2006. "A spacetime discontinuous Galerkin method for elastodynamics with element-level balance of linear momentum". *Computer Methods in Applied Mechanics and Engineering,* ***195***, pp. 3247–73.

[33] Abedi, R., Chung, S.-H., Erickson, J., Fan, Y., Garland, M., Guoy, D., Haber, R., Sullivan, J. M., Thite, S., and Zhou, Y., 2004. "Spacetime meshing with adaptive refinement and coarsening". In Proceedings of the Twentieth Annual Symposium on Computational Geometry, SCG '04, ACM, pp. 300–9.

[34] Abedi, R., and Haber, R. B., 2014. "Riemann solutions and spacetime discontinuous Galerkin method for linear elastodynamic contact". *Computer Methods in Applied Mechanics and Engineering,* ***270***, pp. 150–77.

[35] Abedi, R., Hawker, M. A., Haber, R. B., and Matouš, K., 2009. "An adaptive spacetime discontinuous Galerkin method for cohesive models of elastodynamic fracture". *International Journal for Numerical Methods in Engineering,* ***1***, pp. 1–42.

[36] Abedi, R., Haber, R. B., Thite, S., and Erickson, J., 2006. "An *h*–adaptive spacetime–discontinuous Galerkin method for linearized elastodynamics". *European Journal of Computational Mechanics,* ***15***(6), pp. 619–42.

[37] Omidi, O., Abedi, R., and Enayatpour, S., 2015. "An adaptive meshing approach to capture hydraulic fracturing". In The 49th US Rock Mechanics/Geomechanics Symposium. ARMA 15-572.

[38] Olarewaju, J., Ghori, S., Fuseni, A., Wajid, M., et al., 1997. "Stochastic simulation of fracture density for permeability field estimation". In Middle East Oil Show and Conference, Society of Petroleum Engineers.

[39] Huq, F., Brannon, R., and Graham-Brady, L., 2016. "An efficient binning scheme with application to statistical crack mechanics". *International Journal for Numerical Methods in Engineering,* ***105***(1), pp. 33–62.

[40] Karhunen, K., and Selin, I., 1960. *On linear methods in probability theory*. Rand Corporation.

[41] Loéve, M., 1977. *Probability theory*. Springer, New York.